Aerosol Science and Technology, 45:770–784, 2011
Copyright © American Association for Aerosol Research
ISSN: 0278-6826 print / 1521-7388 online
DOI: 10.1080/02786826.2011.560211

An Aerosol Chemical Speciation Monitor (ACSM) for Routine Monitoring of the Composition and Mass Concentrations of Ambient Aerosol

N. L. Ng,[1] S. C. Herndon,[1] A. Trimborn,[1] M. R. Canagaratna,[1] P. L. Croteau,[1] T. B. Onasch,[1] D. Sueper,[1,2] D. R. Worsnop,[1] Q. Zhang,[3] Y. L. Sun,[3] and J. T. Jayne[1]

[1]*Aerodyne Research, Inc., Billerica, Massachusetts, USA*
[2]*CIRES, University of Colorado, Boulder, Colorado, USA*
[3]*Department of Environmental Toxicology, University of California, Davis, California, USA*

Downloaded By: [Sun, Yele] At: 18:48 7 March 2011

We present a new instrument, the Aerosol Chemical Speciation Monitor (ACSM), which routinely characterizes and monitors the mass and chemical composition of non-refractory submicron particulate matter in real time. Under ambient conditions, mass concentrations of particulate organics, sulfate, nitrate, ammonium, and chloride are obtained with a detection limit <0.2 μg/m^3 for 30 min of signal averaging. The ACSM is built upon the same technology as the widely used Aerodyne Aerosol Mass Spectrometer (AMS), in which an aerodynamic particle focusing lens is combined with high vacuum thermal particle vaporization, electron impact ionization, and mass spectrometry. Modifications in the ACSM design, however, allow it to be smaller, lower cost, and simpler to operate than the AMS. The ACSM is also capable of routine stable operation for long periods of time (months). Results from a field measurement campaign in Queens, NY where the ACSM operated unattended and continuously for 8 weeks, are presented. ACSM data is analyzed with the same well-developed techniques that are used for the AMS. Trends in the ACSM mass concentrations observed during the Queens, NY study compare well with those from co-located instruments. Positive Matrix Factorization (PMF) of the ACSM organic aerosol spectra extracts two components: hydrocarbon-like organic aerosol (HOA) and oxygenated organic aerosol (OOA). The mass spectra and time trends of both components correlate well with PMF results obtained from a co-located high resolution time-of-flight AMS instrument.

1. INTRODUCTION

Aerosols play a significant role in altering the chemistry and the radiative balance of the Earth's atmosphere, in reducing visibility, and in adversely affecting human health (Pöschl 2005; Pope and Dockery 2006; IPCC 2007). In order to address aerosol effects on the environment and health, instrumentation capable of reporting the chemical and microphysical properties of ambient particles is needed. From an air quality monitoring standpoint, aerosol instrumentation that is simple to operate, capable of long-term, autonomous, and stable operation with real time results is also desired.

In recent years the Aerodyne Aerosol Mass Spectrometer (AMS) (Jayne et al. 2000; Canagaratna et al. 2007) equipped with quadrupole (Q-AMS) and time-of-flight (C-ToF-AMS and HR-ToF-AMS) (Drewnick et al. 2005; DeCarlo et al. 2006) mass spectrometers has been deployed in numerous field campaigns and has provided a wealth of chemical and microphysical information about ambient aerosol. A compilation of AMS measurements from 37 Northern Hemispheric surface field campaigns, for example, has been used to characterize ambient aerosol composition in urban, rural, and remote locations (Zhang et al. 2007). A key finding from Zhang et al. (2007) is that a large fraction (45% on average) of the ambient non-refractory submicron aerosol mass consists of organic material and the remaining fraction consists of ammonium nitrate, ammonium sulfate, and ammonium chloride. Positive matrix factorization (PMF) of AMS organic aerosol mass spectra (Lanz et al. 2007; Ulbrich et al. 2009) has been used to further characterize the sources and evolution of ambient organic aerosol (OA) (Jimenez et al. 2009; Ng et al. 2010). Two types of OA groups are observed at

Received 15 November 2010; accepted 19 January 2011.

We thank Ken Demerjian, Jim Schwab, Mike Christophersen, Oliver Rattigan, and the DEC group for assistance during the Queens, NYC study. We also thank Oliver Rattigan for the Thermo Scientific Sulfate Particulate Analyzer data. We thank Leah Williams for helpful comments on the manuscript. This work was supported by EPA SBIR Grant EP-D-05-057 and DOE SBIR Grant DE-SC0001673. The analysis of the QC HR-ToF-AMS data was supported by US Department of Energy Office of Science (BER) (grant DE-FG02-08ER64627, DE-SC0002191).

Address correspondence to J. T. Jayne, Aerodyne Research Inc., 45 Manning Road, Billerica, MA 01821-3976, USA. E-mail: jayne@aerodyne.com

Downloaded By: [Sun, Yele] At: 18:48 7 March 2011

most sites: hydrocarbon-like organic aerosol (HOA) and oxygenated organic aerosol (OOA) (Zhang et al. 2007). The HOA component is a surrogate of primary combustion OA (Zhang et al. 2005a; Zhang et al. 2005b; Lanz et al. 2007; Zhang et al. 2007; Ulbrich et al. 2009). The OOA component dominates the organic aerosol mass in most environments and is a surrogate of secondary OA (SOA) (de Gouw et al. 2005; Zhang et al. 2005a; Zhang et al. 2005b; Volkamer et al. 2006; Lanz et al. 2007; Zhang et al. 2007; Herndon et al. 2008). The O:C ratio for HOA is typically less than 0.2, while that for OOA can range from 0.4 to 0.9 (Ng et al. 2010). At some locations, the OOA component can be further deconvolved into to OOA subtypes that differ in volatility and degree of oxidation: low-volatility OA (LV-OOA, average O:C $= 0.73 \pm 0.14$) and semi-volatile OA (SV-OOA, average O:C $= 0.35 \pm 0.14$) (Jimenez et al. 2009; Ng et al. 2010). Other than HOA and OOA, biomass burning OA (BBOA) (Aiken et al. 2009), cooking OA (COA) (Allan et al. 2010; Huang et al. 2010; Sun et al. 2010), and local OA (LOA) (Docherty et al. 2008; Aiken et al. 2009; Sun et al. 2010) are also observed in other studies.

While the research grade AMS provides valuable information about trends in speciated aerosol mass concentrations for applications that require fast time resolution (1 min or less), it is not well suited for routine air quality monitoring applications because it is expensive to own and requires dedicated scientists (usually with advanced degrees) to operate and analyze its multidimensional data. In this manuscript we introduce the Aerodyne Aerosol Chemical Speciation Monitor (ACSM), a new instrument that has many of the capabilities of the AMS but is better suited for monitoring applications. The ACSM is designed and built around the same sampling and detection technology as the state-of-the art research grade AMS systems, but it has lower size, weight, cost, and power requirements than the AMS and is specifically designed to be a stand-alone monitor that is more easily transportable and can operate with minimal user intervention. Much of the reduced complexity is due to the fact that the ACSM does not measure size distributions; only aerosol mass spectra are reported.

This manuscript provides a detailed description of the ACSM instrument, its operating and calibration procedures, and a sample data set that is compared to other mass-based quantitative instruments which include a HR-ToF-AMS, a Particle-into-Liquid Sampler coupled with Ion Chromatograph (PILS-IC) (Weber et al. 2001) and a Thermo Scientific Sulfate Particulate Analyzer (Model 5020i). Although it uses lower cost components that reduce its sensitivity and time resolution compared to the AMS, the ACSM has sufficient sensitivity to operate as a monitoring instrument providing chemically speciated mass loadings and aerosol mass spectra at data rates up to 30 min for typical urban aerosol loadings (several $\mu g/m^3$). The ACSM has been successfully deployed in three field campaigns: DAURE in Montseny, Spain (March 2009, 3 weeks attended operation), SHARP in Houston, TX (April 2009, 6 weeks unattended operation) and Queens College, NY (July 2009, 8 weeks unattended operation). Since the Queens campaign involved more co-located monitoring and research-grade instruments for comparing the ACSM data with, the Queens dataset is used to demonstrate the performance and capabilities of the ACSM.

2. INSTRUMENT DESCRIPTION

The ACSM measures 19″ D × 21″ W × 33″ H, weighs 140 pounds, and requires approximately 300W of power to operate. Two versions of the instrument have been designed: stand alone bench top and a 19" rack mount system. A schematic of the ACSM is shown in Figure 1. It consists of three vacuum chambers that are differentially pumped by turbo pumps (two Varian V301 pumps and one V81 pump or equivalent Pfeiffer turbo pumps, two HP300 and one HP80) and backed by a small diaphragm pump (Vacuubrand, MD1). During operation, an aerodynamic lens (Liu et al. 1995a; Liu et al. 1995b)

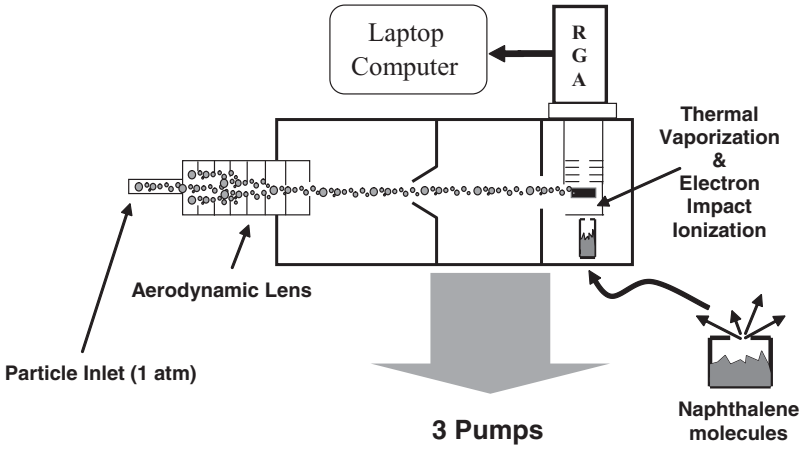

FIG. 1. Schematic of the ACSM. Submicron particles that enter the aerodynamic lens are focused into a narrow beam that impacts a hot vaporizer. The resulting vapor is ionized with electron impact and chemically characterized with an RGA quadrupole mass spectrometer. The detection chamber also contains an effusive source of naphthalene which is used for calibration and routine monitoring of instrument performance (see text for more discussion).

Downloaded By: [Sun, Yele] At: 18:48 7 March 2011

is used to efficiently sample and focus submicron particles into the ACSM. The 50% transmission range of the lens is 75–650 nm (Liu et al. 2007). The sample flow into the instrument, which is fixed by a 100 μm diameter critical aperture mounted at the entrance of the aerodynamic lens, is approximately 85 cc/min. The focused particle beam is transmitted through the first two chambers into the final detection chamber where particles impact and flash vaporize on a hot oven; nonrefractory particulate material that vaporizes at the oven temperature (typically 600°C) is subsequently detected and chemically characterized with 70eV electron impact quadrupole mass spectrometry.

The particle lens and particle vaporizer used in the ACSM are identical to those used in the research grade AMS (Liu et al. 1995b; Liu et al. 1995a; Jayne et al. 2000; Liu et al. 2007). The electron impact ion source used in the ACSM is smaller, but otherwise identical to that used in the AMS (Jayne et al. 2000). Several design features make the ACSM a simpler, smaller, and less expensive stand-alone instrument. Two key design differences include: (1) the use of a lower cost residual gas analyzer (RGA) type quadrupole mass analyzer instead of the high-performance quadrupole and time-of-flight spectrometers used on AMS systems, and (2) the lack of a fast data acquisition and particle beam chopper system for measuring particle time-of-flight to obtain particle size information. Since long particle flight paths are not needed, the overall vacuum chamber length is shorter (14″ vs. 21.5″) and the instrument as a whole only uses 3 turbo pumps rather than the 5 used in AMS systems. Taken together these modifications result in a more compact and less costly instrument compared to the AMS at the expense of lower sensitivity and time resolution.

The RGA employed in the ACSM is the Pfeiffer Vacuum Prisma Plus system. This model is chosen for several reasons. It has good overall sensitivity for its class, 6×10^{-4} amps/mbar (200 amu head). It has a standard cross-beam electron impact ion source compatible with our particle vaporizer source and has easy Ethernet based connectivity via the Open Connectivity standard (OPC). This last fact combined with built in analog and digital control lines allows any computer (including a low end laptop) to be suitable for acquiring the data. No additional data acquisition or I/O cards are required for controlling and automating the ACSM. Data acquisition and control software has been developed using the Microsoft .NET framework. The applied scan rate of the ACSM is chosen to be much slower (0.5–1 s/amu) compared to the Q-AMS (1 ms/amu). The overall sensitivity of the RGA type analyzer is ∼1 order of magnitude lower compared to the high-performance quadrupole used in Q-AMS instruments and ∼2 orders of magnitude lower than the ToF AMS systems. ACSM detection limits are discussed in more detail later in this section.

The detection chamber contains an internal calibration standard that consists of an effusive source of naphthalene (Figure 1). Naphthalene (∼0.2 gm) is put inside a stainless steel container (∼0.5 cc) with a 1 μm pin hole leak (Lenox Laser: http://www.lenoxlaser.com/). The parent peak for naphthalene at *m/z* 128 provides an internal standard for calibrating the mass to charge ratios of the measured ions. Since this source is placed inside the detection chamber, naphthalene is always present in the mass spectra (both background and ambient mass spectra). The naphthalene source also allows for in-situ measurement of the *m/z* dependent ion transmission efficiency of the RGA quadrupole system and allows for routine monitoring of the performance of the instrument and simplified calibration of the ionization efficiency of the mass spectrometer.

The ACSM ion signal must be corrected for contributions from background gases in the detection region of the instrument, including naphthalene from the calibration source. An automated zeroing system as shown in Figure 2a is used to obtain

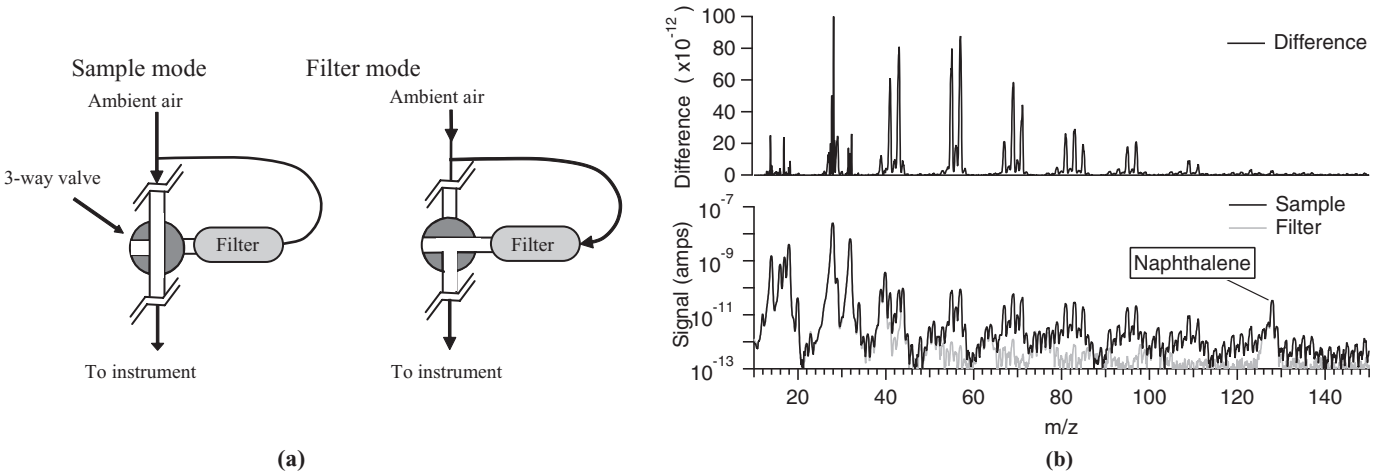

FIG. 2. (a) The 3-way valve system used to automatically measure background signal levels in the ACSM. The valve is switched by the data system to allow ambient air to bypass or pass through a particle filter. As a result the ACSM samples either unperturbed ambient air (sample mode) or particle-free ambient air (filter mode). (b) Examples of ACSM spectra obtained during sample and filter modes. The difference spectrum is obtained by subtracting the filter mode spectrum from the sample mode spectrum.

Downloaded By: [Sun, Yele] At: 18:48 7 March 2011

stable background measurements. Instrument zeroing is done by a 3-way valve system that automatically switches between filter mode and sample mode. In the filter mode, ambient particles are removed from sampled air and the resulting particle-free sample is sent to the ACSM. In the sample mode, ambient aerosol particles are unperturbed and directly sampled into the ACSM. Particle signal is obtain as the difference between the sample and filter mode measurements. Figure 2b shows an example of the sample mass spectrum, filter mass spectrum, and the difference mass spectrum. The chemical species (organics, sulfate, nitrate, ammonium, and chloride (Chl)) measured by the ACSM are determined from the difference mass spectrum following the same methodology used in the AMS as outlined in Allan et al. (2004b). Since signal due to ambient gas phase species (i.e., N_2, O_2, Ar, etc.) is present in both the ambient and filter mode measurements, the automated filter measurements provide an effective way of automatically removing the spectral contributions of ambient gas phase species to the difference spectrum. The ability to cleanly subtract air signals is particularly important in the ACSM, since it has a shorter chamber and thus a more intense molecular air beam than typical AMS instruments.

Figures 3a and b show results from laboratory experiments designed to characterize the detection limits of the ACSM. The ACSM data collection protocol interleaves ambient and particle free measurements. Experiments conducted at shorter time intervals have demonstrated that the instrument response drift is negligible during the typical ambient and particle free modes. An example of data collected where both the "ambient" and particle free measurements were sampling filtered ambient air is depicted in the top panel of Figure 3a. An Allan variance has been performed on the organics time series (lower panel of Figure 3a) in order to quantify sources of instrument drift that are non-random and determine the characteristic time over which data may be averaged to improve signal-to-noise (Werle et al. 1993). Similar analysis is performed for sulfate, nitrate, ammonium, and chloride. Figure 3b shows the 3σ detection limits for each of the species. For 30 min of averaging time (t_{30}), the 3σ detection limits for ammonium, organics, sulfate, nitrate, and chloride are 0.284 μg/m^3, 0.148 μg/m^3, 0.024 μg/m^3, 0.012 μg/m^3, and 0.011 μg/m^3, respectively. Because of the stability of the instrument over time as shown in Figure 3a, the detection limits for longer averaging times (t) can be estimated by multiplying the 30 min detection limit by $\sqrt{t_{30}/t}$. For reference, the 24 h detection limit for ammonium is 0.041 μg/m^3 and the detection limits for all other species are even smaller. It is important to note that this detection limit is ultimately dependent on and will vary with the background mass spectral signal in the ACSM. As can be seen in Figure 3b, detection limits vary for the different species. The highest detection limit is observed for NH_4, whose fragment ions (*m/z* 15, 16, and 17) experience interference from relatively larger background water and oxygen ion fragments.

3. QUANTIFICATION OF AEROSOL MASS

3.1. Theory

Standard AMS instruments have demonstrated that the mass concentration C for a species s can be determined from ion signals at each of its mass spectral fragments i ($I_{s,i}$), and its ionization efficiency (IE_s) as follows (Canagaratna et al. 2007):

$$C_s = \frac{10^{12} MW_s}{IE_s Q N_A} \sum_{\text{all}i} I_{s,i} \quad [1]$$

where C_s is in units of μg/m^3, IE_s is in units of ions/molecule, $I_{s,i,}$ is in units of ions/s, N_A is Avogadro's number, MW_s is the molecular weight of species s, and Q is the volumetric sample flow rate into the instrument in cm^3 s^{-1}. The 10^{12} factor is needed for unit conversion. Since calibration of IE_s for all ambient species s is not feasible, IE_s is expressed in terms of the IE of the NO_3 moiety of calibration with NH_4NO_3 particles as

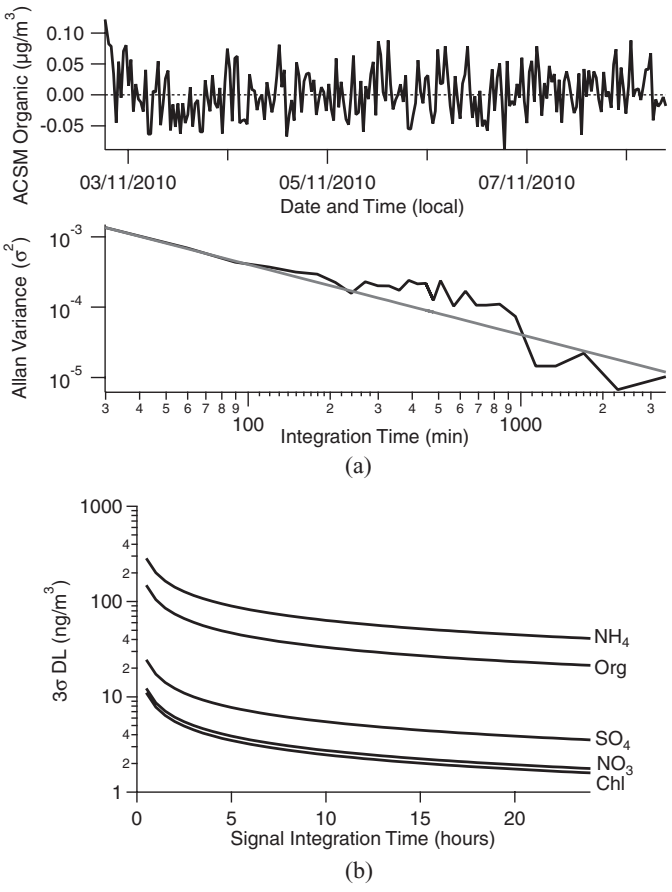

FIG. 3. (a) Allan variance analysis. The upper panel depicts the organic mass loading as a function of time (top axis) while the lower panel is the result of the Allan variance calculation. The Allan variance result (black line) follows a theoretical drift free instrument containing only white noise (gray line). (b) Three sigma detection limits for the non-refractory species detected by the ACSM as a function of signal integration time. The detection limits are ultimately dependent on the background levels in the ACSM.

follows:

$$\frac{IE_s}{MW_s} = RIE_s \frac{IE_{NO3}}{MW_{NO3}} \quad [2]$$

where RIE_s is the relative ionization efficiency of species s, compared to NO_3 (Jimenez et al. 2003). The *RIE* values usually used in AMS ambient concentration calculations are 1.4 for organic molecules and 1.1, 1.15, and 3.5–6 for NO_3, SO_4, and NH_4 moieties, respectively (Canagaratna et al. 2007). The RIE_{NO3} is greater than 1 because the calibrations monitor NO^+ and NO_2^+ which together account for only 90% of the total ion signal from the NO_3 group (nitrogen and oxygen atoms are not monitored due the poor signal-to-background levels at these masses). IE_{NO3} and RIE_{NH4} can be directly calibrated during the NH_4NO_3 calibrations (see calibration section below for more details).

In the standard AMS systems, the high time resolution detection electronics allow for precise measurements of single ions and single particles, and thus $I_{s,i}$ and IE_{NO3}. With the ACSM, however, direct measurements of single particles are not possible owing to the slower detection electronics (no capability to time resolve single ions). Thus, in practice, calibration of the ACSM is based on determining an instrument response factor, *RF*, using NH_4NO_3 calibration aerosol. A known aerosol loading is sampled with a combination of differential mobility analyzer (DMA) and condensation particle counter (CPC) and the sum of the ion signals representing the NO_3 moiety is recorded with the ACMS. RF_{NO3} is measured in units of amps of signal per $\mu g/m^3$ of sampled aerosol. When normalized to the calibration volumetric sample flow rate Q_{cal} (in units of cm^3 s^{-1}) and multiplier gain G_{cal} (~20,000), RF_{NO3} is proportional to the ionization efficiency of NO_3 (in units of ions/molecule) as follows:

$$IE_{NO3} * \frac{N_A}{MW_{NO3}} = \frac{RF_{NO3}}{Q_{cal} G_{cal}} \quad [3]$$

The flow is proportional to the aerodynamic lens pressure which is measured continuously with a 10 Torr baratron gauge (MKS Instruments). The relationship between inlet flow and lens pressure is calibrated by measuring the lens pressure for a series of known inlet flows. In the ACSM direct determination of the multiplier gain is also not possible owing to the slow detection electronics. Thus, the gain is estimated based on the measured ratio of the electron multiplier signal to the Faraday cup signal (raw ion current) for a particular ion, typically *m/z* 28. During *RF* calibration (and operation), the multiplier voltage in the ACSM is set so that the gain is ~20,000. This (relatively low) gain value is chosen to maximize the multiplier lifetime in the instrument.

Combining Equations (1)–(3) yields the ACSM equation for obtaining mass concentrations of species s from measured ion current, *IC* (in amps), at fragments i as follows:

$$C_s = \frac{CE}{T_{m/z}} * \frac{10^{12}}{RIE_s} \frac{Q_{cal} G_{cal}}{RF_{NO3}} \frac{1}{QG} \sum_{\text{all}i} IC_{s,i} \quad [4]$$

Equation (4) also includes corrections for the *m/z* dependent ion transmission efficiency of the quadrupole ($T_{m/z}$) and the non-unit particle collection efficiency (CE) of the ACSM (see below). In general, operating values for Q and G are similar to their respective values during calibration (Q_{cal} and G_{cal}) and so these parameters effectively cancel each other out in Equation (4).

A disadvantage of the use of the smaller lower cost quadrupole is the inherent performance limitation owing to reduced ion transmission through the analyzer as larger mass-to-charge ratios are filtered. The Prisma Plus RGA used here has 6 mm diameter quadrupole rods and a 200 amu range. Over this range, we observe a decrease in ion transmission of approximately a factor of five and corrections for this performance limitation need to be applied. As discussed in Section 3.3., the internal naphthalene standard provides a means to monitor and determine the ion transmission.

Finally, aerosol mass concentrations need to be corrected for particle collection efficiency. CE values can be less than 1 owing to (a) shape-related collection losses at the vaporizer from inefficient focusing of non-spherical particles, (b) particle losses at the vaporizer due to bouncing of solid particles before they are completely vaporized, and (c) particle losses in the aerodynamic inlet as a function of particle diameter (Huffman et al. 2005; Canagaratna et al. 2007; Liu et al. 2007; Matthew et al. 2008). Current ACSM systems use the identical aerodynamic lens and vaporizer design used in AMS systems so we expect CE values are similar to those observed in AMS measurements. The large database of AMS field results indicates that a CE value of 0.5 reproduces speciated AMS mass concentrations for ambient particles to within 25% of those measured by collocated instruments (Canagaratna et al. 2007). Higher CE values have been observed for pollution events containing ambient aerosol with high NH_4NO_3 content, high levels of sulfate acidity, or large amounts of liquid H_2O (Canagaratna et al. 2007 and references therein).

3.2. Calibrations

Ammonium nitrate is used as the calibration aerosol because it is well focused by the aerodynamic lens (all particles reach the vaporizer) and it vaporizes with 100% efficiency (CE = 1). Thus, it provides a quantitative source of NO_3 (and NH_4) ions. Since the ACSM does not have fast detection electronics to time-resolve single particle pulses, the measured NO^+ and NO_2^+ nitrate signals are averaged over many calibration particles and compared with the input mass of NO_3. Briefly, mono-disperse ammonium nitrate particles, generated with an atomizer, passed through a diffusion dryer and size selected with a DMA, are delivered into both the ACSM and a CPC. With the

Downloaded By: [Sun, Yele] At: 18:48 7 March 2011

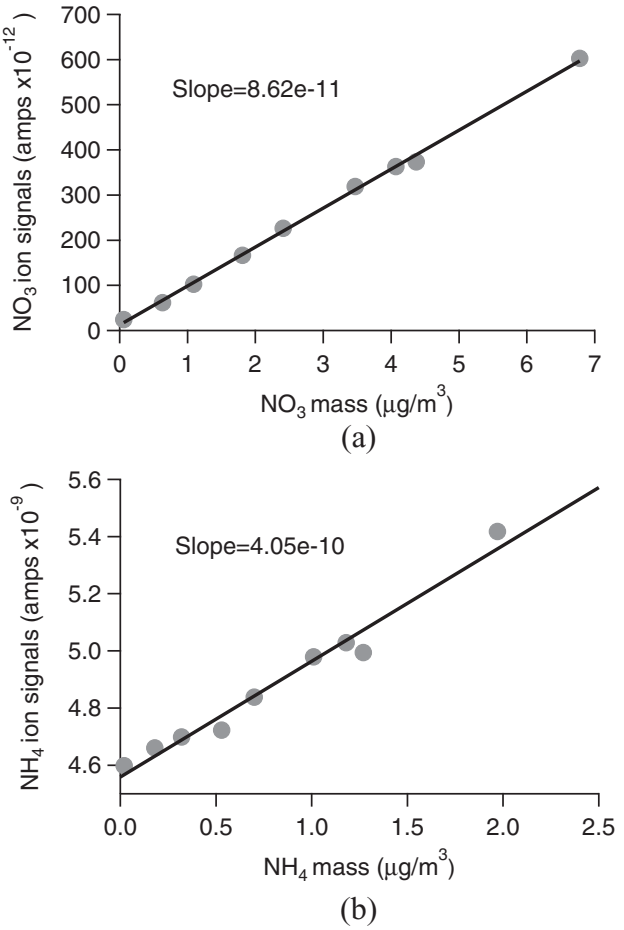

FIG. 4. Measurements of ACSM response factors for NO_3 and NH_4. Ion signals are measured as a function of known input mass concentrations of NO_3 and NH_4. The slopes of these graphs correspond to the response factors of interest. Size selected (300 nm) NH_4NO_3 calibration particles are used for the measurements.

known particle size and number concentrations of the particles, the mass of the particles can be calculated (Jayne et al. 2000; Jimenez et al. 2003). Figure 4 shows an example of RF_{NO3} and RF_{NH4} measurements. The nitrate and ammonium ion signals measured (in amps) are plotted against the calculated nitrate and ammonium masses from the DMA/CPC combination. The use of an aerosol dilution system provides a convenient way to vary the input mass concentration. The slope of the lines in Figures 4a and b is the *RF* for each species and will depend on the precise value of *G* and *Q*. The ratio of RF_{NH4}/RF_{NO3} is RIE_{NH4}. Typically, this calibration is performed using calibration particles with 300 nm mobility diameters. Care must be taken to avoid using calibration particles that do not have unit transmission through the aerodynamic lens since this will result in *RF* values that are biased low. Calibrations particles that are small and contain a significant fraction of multiply charged particles (with equivalent mobility diameter) in the DMA output, on the other hand, bias the *RF* values high. Equivalent calibration results obtained over several size ranges are used to confirm that neither of these effects bias the results. For an ammonium nitrate solution of ~5 mM (using TSI model 3076 constant output atomizer) and size-selected 300 nm mobility diameter particles, it is found that the mass contribution of multiply charged particles is negligible. The calibration accuracy will be limited by the accuracy of the DMA and CPC instruments as well.

After a calibration is performed, the reference state of the instrument is defined and any relative changes in the internal standard naphthalene signal at *m/z* 128 as well as the air ion signals from the reference state can be used to monitor changes in overall detector performance (naphthalene and/or air) or changes due to variation in the sampling flow rate (air only). The effusive rate of the naphthalene depends on the pin hole size, which in this case is 1 μm diameter, as well as the temperature dependent vapor pressure of the material. The vapor pressure, and hence the naphthalene ion signal, therefore depends on the temperature of the source which will vary with the vacuum chamber temperature. The chamber temperature is routinely monitored for this reason. The variation in naphthalene signal with chamber temperature follows the Clausius-Clapeyron equation as shown in Figure 5a. The slope and intercept of the fit can be used to calculate the temperature-corrected naphthalene signal as shown in Figure 5b. The variability in the temperature-corrected naphthalene signal over the course of the measurement shown in Figure 5b provides an indication of the temporal variation in the gain of the electron multiplier (*G*) and/or *RF*. Mass concentrations can be corrected using the temperature corrected naphthalene signal. We note here that the naphthalene source might also be used as an internal standard for determining instrument *RF*, however, at this stage of development this remains to be demonstrated.

3.3. Ion Transmission Correction

As shown in Equation (4), values for $T_{m/z}$ are needed for ACSM mass concentration calculations. The transmission efficiency of the RGA quadrupole drops off sharply as a function of *m/z* beyond a low *m/z* range where it is relatively constant. Since the naphthalene spectrum is always present in the background ACSM spectra, $T_{m/z}$ is monitored routinely by comparing the observed naphthalene fragmentation pattern to the 75 eV electron impact spectra in the NIST database (http://webbook.nist.gov/). Figure 6 shows an example of the RGA mass dependent transmission efficiency observed for the ACSM deployed during the Queens College, New York campaign discussed below. Naphthalene fragment ion peaks with intensities >~1% of the parent ion occur in the 50 s, 60 s, 70 s, 100 s, and 120 s mass ranges, and the ratios of the sums of peaks intensities in these decades to those in the NIST fragmentation pattern are used to determine $T_{m/z}$, setting the *m/z* (50 + 51) peaks to a reference transmission efficiency of 1. Agreement is also seen using the naphthalene fragmentation pattern measured on the higher performance quadrupole (16 mm diameter rod system, Pfeiffer Vacuum QMA 410). The naphthalene-based transmission efficiency curve is in

Downloaded By: [Sun, Yele] At: 18:48 7 March 2011

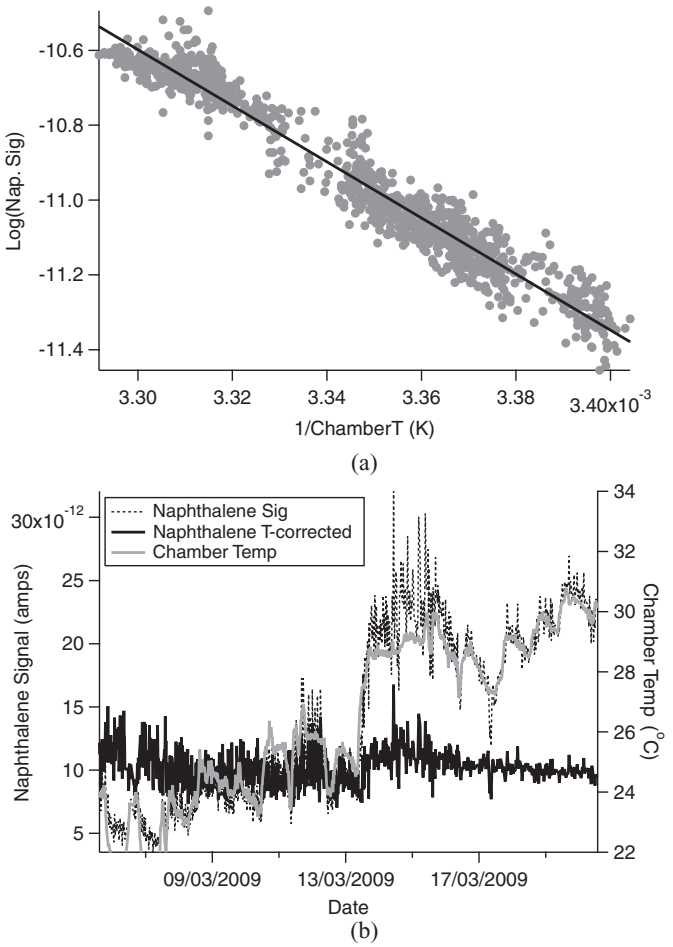

FIG. 5. (a) Variation in naphthalene signal with chamber temperature. (b) Time trends of raw and temperature corrected naphthalene signals. Temperature corrected naphthalene signals are obtained using the relationship observed in Figure 4a.

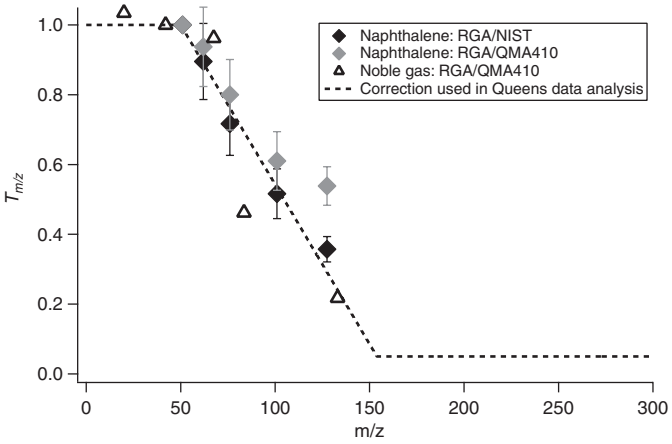

FIG. 6. *m/z* dependent ion transmission efficiency ($T_{m/z}$) of the RGA quadruple. $T_{m/z}$ is monitored routinely by comparing the ratio of the observed naphthalene fragmentation pattern to the 75 eV electron impact spectra in the NIST database. Agreement is also seen using the naphthalene fragmentation pattern measured on the higher performance Pfeiffer quadrupole (QMA 410). The naphthalene-based transmission efficiency (described by the dotted line) is in reasonable agreement with the measurements using a standard gas mixture with known concentrations of different noble gases. The error bars are one standard deviation of the calculated point-by-point transmission efficiency for the entire Queens dataset.

reasonable agreement with the measurements using a standard gas mixture with known concentrations of different noble gases (Ne, Ar, Kr, Xe). In this case, the noble gases were measured using both the ACSM (6 mm diameter rod system) and the higher performance quadrupole. We have described the mass dependant transmission to be unity up to *m/z* 50, then a linear decrease with a slope of −0.009 up to about *m/z* 150. In practice, there is very little particle mass observed above ∼*m/z* 100 and for this reason we have limited the drop off to 0.05 at ∼*m/z* 150 (a 20× correction) so as to avoid large correction errors.

It is important to note that the precision of the naphthalene-based transmission efficiency measurement can be affected by background gas signals that interfere with the naphthalene fragment ions. The variability at each data point of the transmission efficiency measurements in Figure 6, in fact, reflects the temperature dependent variation in non-naphthalene background ion signals at *m/z* 50 and 51 which were used to normalize the higher mass peak intensities. We note that the transmission efficiency of identical quadrupoles can vary with resolution and tuning parameters and would not be expected to be identical to that shown in Figure 4. Hence, the internal standard provides an in-situ correction for individual instruments.

4. FIELD MEASUREMENTS

4.1. General Information

The Queen College Air Quality Study took place at Queens College, New York (Coordinates: 40.73614 N -73.82153 W), which is a highly populated residential area and is less than 1 km south of the Long Island Expressway (I-495) and approximately 1 km east of the Van Wyck Expressway (I-678), two of the busiest highways in New York City. The field campaign (involving multiple gas and particle instruments) was conducted from July 13 to August 4, 2010 (Sun et al. 2010). After the 3-week campaign, the ACSM continued to sample unattended through September 9, 2010 (i.e., 8 weeks deployment in total). There are two main sampling locations for this study. The first one is at the New York State Department of Environmental Conservation (NYS DEC) air monitoring building, which is one of the sites in the Chemical Speciation Network (CSN) operated by the EPA. The ACSM was located in this building. The air monitoring building is equipped with a comprehensive set of instruments for measuring $PM_{2.5}$ mass and composition as well as gas-phase pollutants (e.g., CO, NO_x, O_3, SO_2, etc.). The building is maintained at 22°C. The second location is at the parking lot #6 of the campus, which is approximately 100 m south of the air monitoring building. The Atmospheric Sciences Research Center (ASRC), University at Albany mobile laboratory was parked at this location. The door of the ASRC mobile

Downloaded By: [Sun, Yele] At: 18:48 7 March 2011

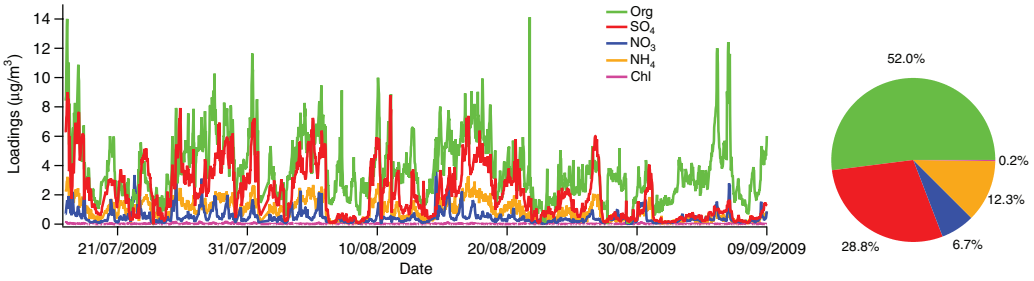

FIG. 7. Time trends of non-refractory submicron aerosol species measured with the ACSM during the Queens, NY study. Mass concentrations are calculated with a collection efficiency of 1 for all species. The average total loading is 7.2 μg/m^3. The time resolution of these measurements is 30 min. The ACSM operated unattended during this study.

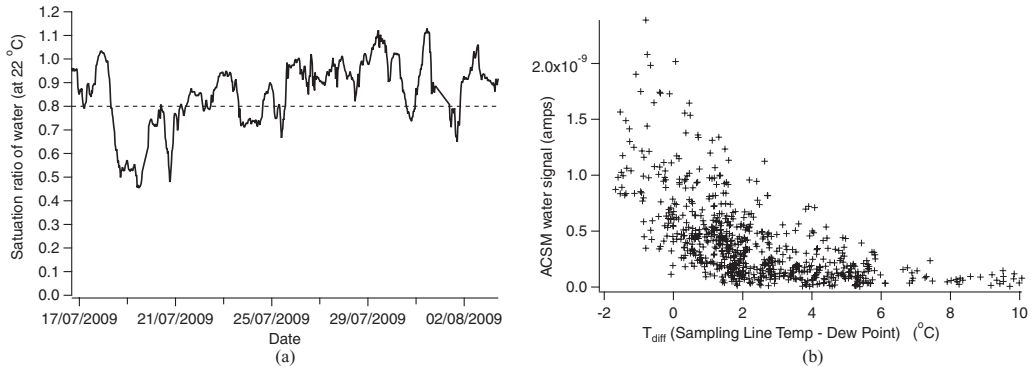

FIG. 8. (a) Saturation ratio of water in the sampling inlet line of the ACSM during the Queens study. The large saturation ratios >0.8 indicate that water condensation in the sampling line was likely. (b) ACSM water signal as a function of difference between sampling line temperature and the ambient dew point. When the temperature difference was <5°C, clear ACSM particle water signal was observed.

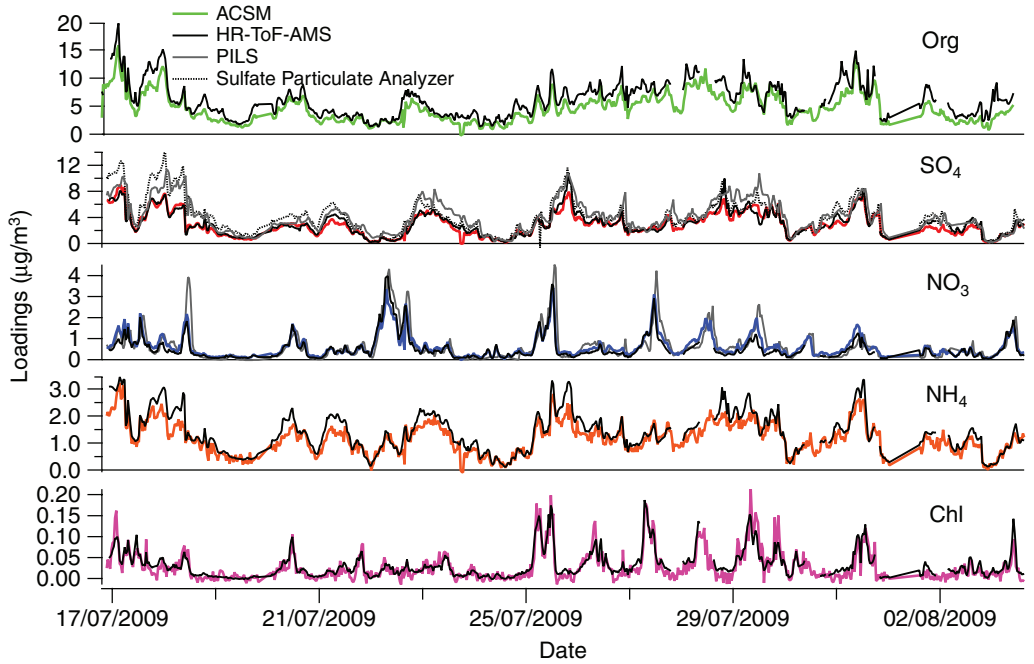

FIG. 9. Speciated ACSM time trends observed during the Queens study. These trends agree well with data from collocated instruments (PILS-IC, Thermo Scientific Sulfate Particulate Analyzer Model 5020i, and HR-ToF-AMS). Note: Color traces are ACSM data.

Downloaded By: [Sun, Yele] At: 18:48 7 March 2011

laboratory was open most of the time and hence sampling was conducted at ambient temperature and RH.

The main instruments for comparing the ACSM data with are the Aerodyne high-resolution time-of-flight AMS (HR-ToF-AMS) (DeCarlo et al. 2006) owned and operated by the SUNY Albany group, a PILS-IC, and a Thermo Scientific Sulfate Particulate Analyzer. During the field campaign, the HR-ToF-AMS was located inside the ASRC mobile laboratory at the parking lot and the ACSM, PILS-IC, and the Thermo Scientific Sulfate Particulate Analyzer were located inside the air monitoring building. Ambient air was drawn into ACSM through a 3/8" OD copper tube extending ~2 m above the roof top. Coarse particles were removed using a cyclone with 2.5 μm cut off (URG Model 2000-30EN operating at 10 LPM flow rate). The residence time in the sampling tube was 1.5 s.

The ACSM data reported here is in UTC. The local time during this study is Eastern Daylight Saving Time (EDT = UTC–4 h).

4.2. Total Submicron Aerosol: Mass Concentrations and Time Series

The ACSM ran unattended continuously for 8 weeks with a 30 min sampling time interval. The data were uploaded to an FTP site automatically each time a new file was written. Shown in Figure 7 are the time series of organics, sulfate, nitrate, ammonium, and chloride as well as the average mass fraction of each species measured by the ACSM. The concentrations are reported with CE of 1 (further explained below). They have also been adjusted based on the temperature-corrected naphthalene signal and the fluctuations in inlet flow rate. The average total loading is 7.2 $\mu g/m^3$; the aerosol is dominated by organics and sulfate species throughout the campaign, with organics accounting for more than 50% of the aerosol.

A more detailed report of chemical composition, size distributions, elemental composition, and temporal variations of non-refractory chemical species in submicron particles as measured by the HR-ToF-AMS during the Queen College Air Quality Study are presented in Sun et al. (2010). In this work, we will mainly focus on the comparison of time series of the chemical species and OA components measured by the ACSM and the HR-ToF-AMS.

As mentioned earlier, the ACSM was located inside the air monitoring building which was maintained at 22°C. However, the outside temperature and RH were much higher; for some days the temperature was as high as 32°C, and the average RH throughout the campaign was 75% (Sun et al. 2010). The saturation ratio of water vapor (at 22°C) is calculated based on the ambient temperature and RH data and is shown in Figure 8a. Laboratory experiments (Matthew et al. 2008) and field measurements (Allan et al. 2004a) indicate that when the RH in the sampling line is >0.8, water condenses onto particles and the particle CE is unity. Since the saturation ratio calculated in the ACSM sampling line is >0.8 most of the time (average = 0.85), a CE of 1 has been applied to the ACSM data. The high water content of the aerosol is further supported by examining the particle water signal measured by the ACSM. Figure 8b shows the water signal measured by the ACSM as a function of the difference (T_{diff}) of the sampling line temperature (i.e., 22°C) and the dew point temperature (calculated based on ambient temperature and RH). It is clear that for $T_{diff} < 5$°C, water is always present in the particles, indicating the particles are likely to be liquid and would have a high CE. This is consistent with the AMS observations in Allan et al. (2004a), in which the measured sulfate concentration was enhanced due to deliquescence for $T_{diff} < 5$°C.

The concentrations of the different species measured by the ACSM are compared to those measured by HR-ToF-AMS (Figure 9) in Sun et al. 2010. The scatter plots of different species are shown in Figure 10. In general, there is very good correlation between the ACSM and HR-ToF-AMS data (R^2 = 0.81–0.91, slope = 0.76–1.01). The organic mass concentrations measured by ACSM are relatively lower than those measured by HR-ToF-AMS and will be discussed later (Section 4.3). For sulfate, other than the HR-ToF-AMS, two other comparison instruments are present at the shelter: PILS-IC and Thermo Scientific Sulfate Particulate Analyzer. Both the PILS-IC and the Thermo Scientific Sulfate Particulate Analyzer measure $PM_{2.5}$ sulfate. Comparing the Sulfate Particulate Analyzer data to 24-h integrated (1 in 3 days sample collection) nylon filter sulfate collected by the Met One Spiral Aerosol Speciation Sampler (SASS) shows that the Sulfate Particulate Analyzer data are biased low. Hence, the Sulfate Particulate Analyzer data is divided by a "recovery" factor of 0.7 (Personal communication, Oliver Rittagan, James Schwab; Schwab et al. 2006). The sulfate aerosol mass measured by the ACSM agrees well with measurements from these three independent instruments (R^2 = 0.91, 0.77, 0.85, slope = 0.95, 0.69, 0.69, for HR-ToF-AMS, PILS-IC, and Sulfate Particulate Analyzer, respectively). The ACSM nitrate data also agree with the PILS-IC data (R^2 = 0.65, slope = 0.75). The ACSM sulfate and nitrate account for ~70% of those in $PM_{2.5}$ measured by PILS-IC (Sun et al. 2010) and Sulfate Particulate Analyzer.

4.3. Investigating OA Components with Positive Matrix Factorization (PMF)

We apply PMF analysis to the ACSM Queens dataset. The PMF2 executable version 4.2 is used in robust mode together with a custom software tool for solution comparison and analysis, the PMF Evaluation Tool (PET) (Ulbrich et al. 2009). The analysis and input error matrix calculations are performed following the procedures described in Ulbrich et al. (2009). Several criteria are employed to determine the optimum number of factors: the scaled residuals are examined carefully, the mass fractions and diurnal cycles of each factor are evaluated and compared, time series are compared to external tracers (including O_3, NO_x, SO_2, NO_3^-, and SO_4^{2-}), and factor spectra are compared to source mass spectra from the AMS MS database (Ulbrich et al. 2009). The uncertainty of the solutions can be examined by running the PMF algorithm from different starting

Downloaded By: [Sun, Yele] At: 18:48 7 March 2011

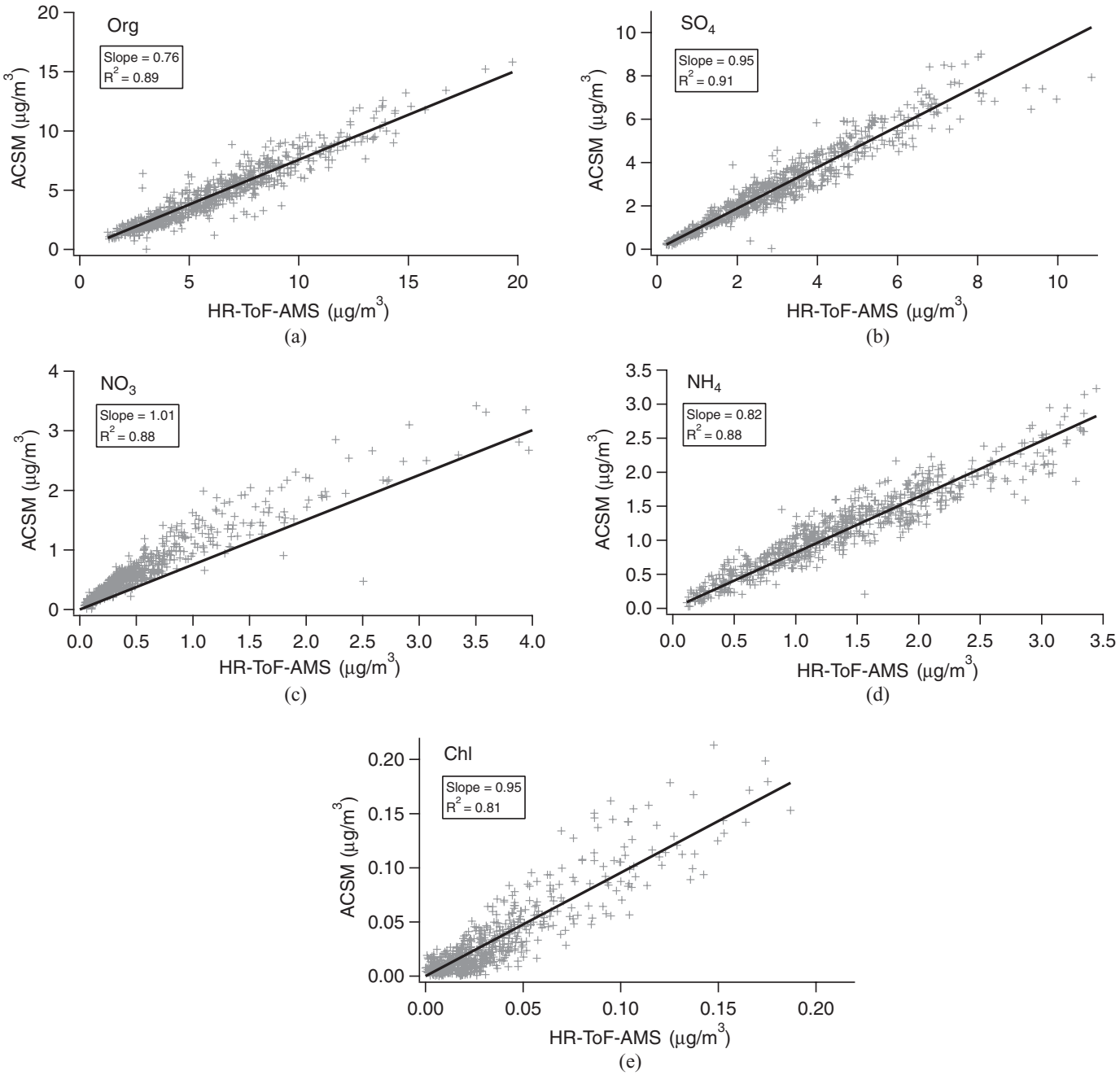

FIG. 10. Scatter plots between the speciated mass concentrations measured by ACSM and HR-ToF-AMS for organics, sulfate, nitrate, ammonium, and chloride.

points (SEED parameter). Rotational ambiguity can be explored by examining the appearance and disappearance of zero values in the mass spectra and time series of the factors through changing the FPEAK parameter (Paatero 2008; Ulbrich et al. 2009). A priori information about component time points or fragment ions with true zero values is not known in typical ambient datasets. Thus, the appearance of unrealistic zero values in the mass spectra and time series of the solutions can be used to evaluate the most reasonable limits of the FPEAK parameter (Ulbrich et al. 2009). Overall, the effect of positive FPEAK is to create more near-zero values in the mass spectra and decrease the number of near-zero values in the time series; negative FPEAK values have the opposite effect (Ulbrich et al. 2009). For the Queens dataset, the analysis is repeated by using different SEED values (while keeping FPEAK constant at 0) and varying FPEAK values from –1 to 1 (while keeping SEED constant at 1). It is found that the component mass spectra and time series do not vary drastically with the SEED value; a SEED value of 1 is used for this dataset. A 3-factor solution (1 HOA and 2 OOA components) with FPEAK = 0.2 is chosen for the ACSM Queens dataset

Downloaded By: [Sun, Yele] At: 18:48 7 March 2011

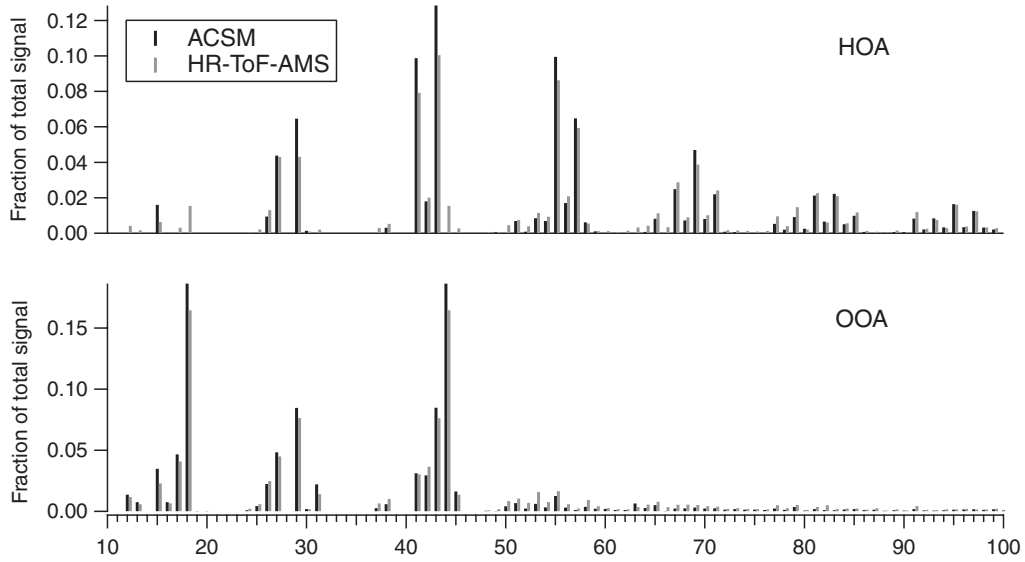

FIG. 11. HOA and OOA component mass spectra extracted with PMF from the Queens ACSM dataset. Similar components are extracted with unit mass resolution PMF analysis of HR-ToF-AMS organic data, and their spectra are also shown for comparison.

Downloaded By: [Sun, Yele] At: 18:48 7 March 2011

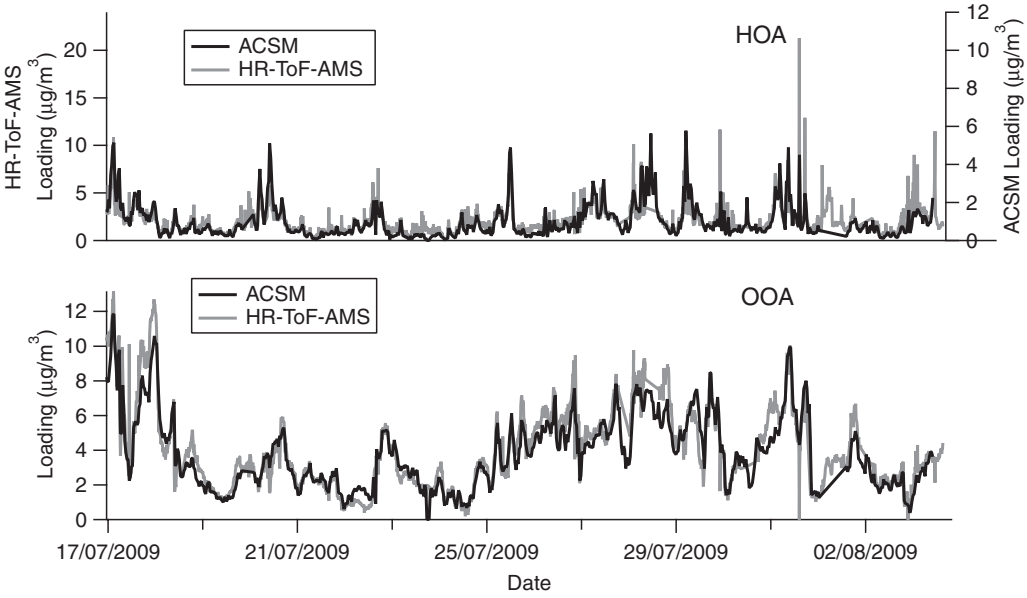

FIG. 12. HOA and OOA component time series extracted from the Queens ACSM dataset. The time trends of these components are similar to those of the HOA and OOA components extracted from unit mass resolution PMF analysis of the HR-ToF-AMS organic data.

after considering the criteria mentioned above. For the purpose of this analysis, the two OOA components were recombined into a single OOA factor. The mass spectra and times series of each component are shown in Figures 12 and 13, respectively. The HOA component is distinguished by the clear hydrocarbon signatures in its spectrum, which are dominated by the ion series $C_nH^+_{2n+1}$ and $C_nH^+_{2n-1}$ (*m/z* 27, 29, 41, 43, 55, 57, 69, 71, 83, 85, 97, 99...) that are typical of hydrocarbons. The OOA component is distinguished by the prominent *m/z* 44 (CO_2^+) in its spectrum and the lower relative intensity of higher mass fragments. The f_{44} (ratio of *m/z* 44 to total signal in the component mass spectrum) in the OOA spectrum is 19%, which is at the high end of the f_{44} observed in the OOA components observed across multiple sites around the world (Jimenez et al. 2009; Ng et al. 2010).

The unit mass resolution PMF results for the HR-ToF-AMS data (Sun et al. 2010) are also shown in Figures 11 and 12. There is good agreement between the mass spectra and time

Downloaded By: [Sun, Yele] At: 18:48 7 March 2011

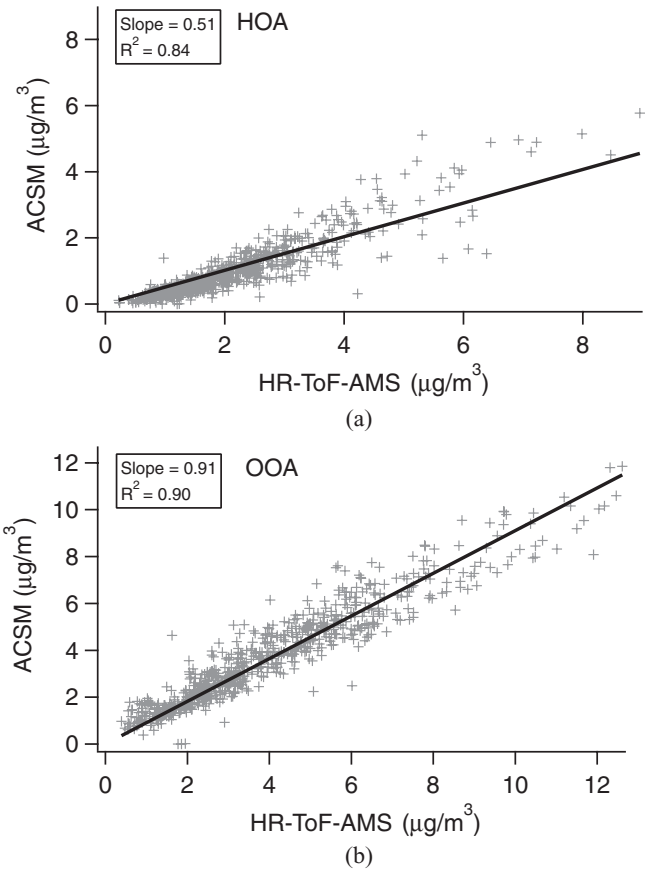

FIG. 13. Scatter plots of HOA and OOA mass concentrations observed with the ACSM and HR-ToF-AMS instruments. The different slopes observed for the two components indicate that they are collected in the ACSM with different collection efficiencies (see text for more discussion).

series of both the HOA and OOA components determined from the ACSM and HR-ToF-AMS data. The scatter plots of the HOA and OOA time series are shown in Figure 13. The OOA loading agrees well between the two instruments, but the HOA loading determined from the ACSM data is approximately half of that determined from the HR-ToF-AMS data, As discussed earlier, a CE of 1 was applied to the ACSM data to account for water condensation on the particles in the sampling line. While a CE of 1 results in good agreement for the OOA component and the inorganic species, it appears that the HOA component is measured with a lower CE (~0.5) in the ACSM. Different CE values could results from different degrees of water uptake for particles containing HOA and OOA components. Recently, Chang et al. (2010) postulated that the degree of oxidation governs the hygroscopicity of the aerosol: the oxygenated OA component contributes to aerosol hygroscopicity while the non-oxygenated OA component does not. HOA is hydrocarbon like and is aliphatic in nature; it has been shown in laboratory experiments that such type of compounds are not CCN-active (Raymond and Pandis 2002; Kumar et al. 2003). Moreover, in ambient measurements where HOA is high, the organic component does not appear to contribute to the CCN-activity (Broekhuizen et al. 2006; Cubison et al. 2008; Quinn et al. 2008). On the other hand, OOA is highly oxidized (with a high O:C) and it has been shown that the organic aerosol becomes more hygroscopic with increasing O:C (Jimenez et al. 2009; Massoli et al. 2010).

Mass weighted HR-ToF-AMS particle size distributions measured during different times of the day provide further evidence that the HOA component is externally mixed. As seen in Figure 14, the organic size distribution has two modes in the morning when there is substantial HOA contribution, an accumulation mode and a smaller mode. This bimodal distribution of organics has been observed in multiple ambient measurement campaigns (Canagaratna et al. 2004) including the 2001 Queens New York Study (Drewnick et al. 2004). The smaller particle mode has a vacuum aerodynamic size that is similar to freshly emitted primary fractal particles (Canagaratna et al. 2004), is externally mixed from inorganic species, and largely consists of

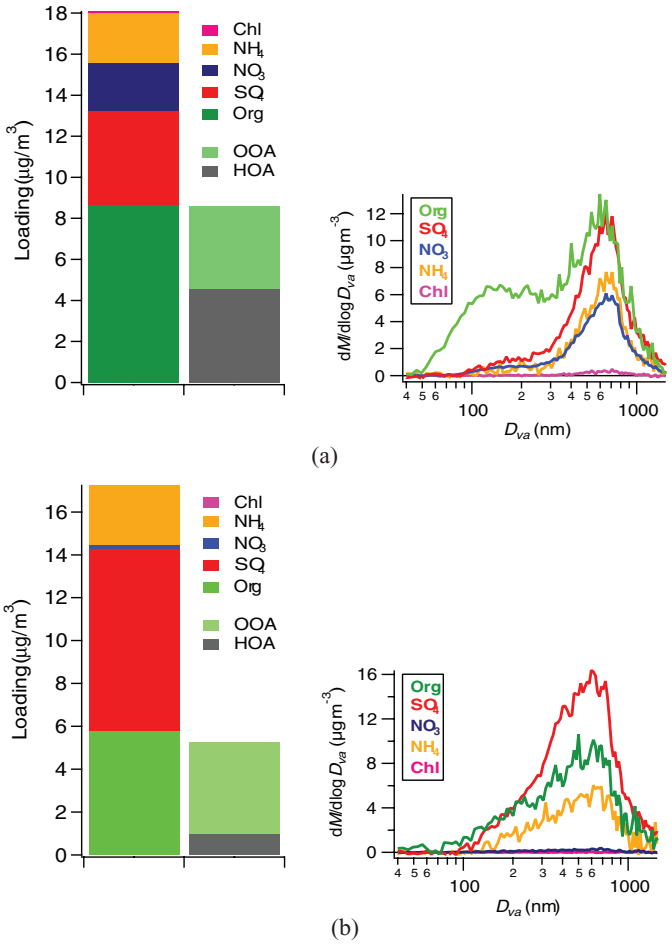

FIG. 14. Mass-weighted size distribution measured with the HR-ToF-AMS during the Queens study. During morning time periods when primary traffic emissions are high (high HOA concentrations), a small externally mixed particle mode is observed. In the afternoon, when the organic loading is dominated by OOA, the organic and inorganic species appear to be internally mixed with each other.

HOA species (Sun et al. 2010). The accumulation mode, on the other hand, is most intense in the afternoon hours when the organic aerosol mass is dominated by OOA. The similarity of the organic and inorganic accumulation mode distributions further indicates that they are internally mixed. Taken together, these observations are consistent with the hypothesis that externally mixed HOA particles have a CE of ∼0.5 because they remain dry in the humid sampling inlet, while OOA, which is internally mixed with inorganic species, has a CE of 1 because it is more hygroscopic and takes up enough water in the sampling line to become liquid.

5. CONCLUSIONS

This manuscript introduces the Aerodyne Aerosol Chemical Speciation Monitor (ACSM), an instrument that is designed for long-term, autonomous, and stable field measurements of ambient aerosol. The ACSM operates by sampling ambient aerosol through an aerodynamic inlet, vaporizing them on a hot oven, and then analyzing the resulting vapor with electron impact ionization quadrupole mass spectrometry. The ACSM is based on the widely used Aerodyne aerosol mass spectrometer (AMS), but key changes in the detection electronics and mass spectrometer allow the ACSM to be smaller, lower cost, and simpler to operate. The ACSM is not designed to measure size distributions. Although these changes lower the relative sensitivity of the ACSM, it still has a detection limit of $< 0.2\ \mu g/m^3$ for 30 min of averaging, which is suitable for measuring typical urban aerosol loadings of several $\mu g/m^3$. The similarities with the AMS allow ACSM data to be analyzed with and profit from all the methods that already have been and continue to be developed for the AMS. The ACSM has been deployed in 3 different field campaigns. Results from the Queens campaign, where it operated continuously and unattended for 8 weeks, are used to demonstrate the performance and capabilities of the ACSM. During the campaign the ACSM provided real-time (30 min resolution) chemically resolved mass concentrations of particulate ammonium, nitrate, sulfate, chloride, and organic species. PMF analysis of ACSM organic spectra is used to further speciate the observed organic aerosol material into HOA and OOA components. The inorganic measurements agree well with those obtained from other aerosol mass instrumentation (PILS-IC, Thermo Scientific Sulfate Particulate Analyzer). The speciated inorganic aerosol time trends and organic aerosol components also compare well with results from a co-located HR-ToF-AMS instrument. Detailed analysis indicates a difference in the effective ACSM collection efficiency factors for HOA and OOA due to the unusually humid (RH > 0.8) conditions of the sampling inlet used during this campaign. In the humid inlet, hygroscopic aerosol particles containing inorganic species and OOA appear to take up liquid water and are collected with a CE of 1 on the ACSM vaporizer. HOA containing particles, on the other hand, are externally mixed from OOA and inorganic species. They are not very hygroscopic and thus they appear to remain dry and are collected in the ACSM with a CE of 0.5 even under the humid sampling inlet conditions. In ambient sampling applications with the ACMS (and the AMS) we recommend drying the aerosol sample to levels well below 80% RH to avoid the potential of a variable CE due to RH variations. For example, Nafion drying tubes are often used to control the humidity of the sampling line. In the future, this and/or other methods should be used to eliminate the complicating inlet effects due to particle composition dependent water uptake that were observed during this study.

REFERENCES

Aiken, A. C., Salcedo, D., Cubison, M. J., Huffman, J. A., DeCarlo, P. F., Ulbrich, I. M., Docherty, K. S., Sueper, D., Kimmel, J. R., Worsnop, D. R., Trimborn, A., Northway, M., Stone, E. A., Schauer, J. J., Volkamer, R. M., Fortner, E., de Foy, B., Wang, J., Laskin, A., Shutthanandan, V., Zheng, J., Zhang, R., Gaffney, J., Marley, N. A., Paredes-Miranda, G., Arnott, W. P., Molina, L. T., Sosa, G., and Jimenez, J. L. (2009). Mexico City Aerosol Analysis During MILAGRO Using High Resolution Aerosol Mass Spectrometry at the Urban Supersite (T0)—Part 1: Fine Particle Composition and Organic Source Apportionment. *Atmos. Chem. Phys.* 9:6633–6653.

Allan, J. D., Bower, K. N., Coe, H., Boudries, H., Jayne, J. T., Canagaratna, M. R., Millet, D. B., Goldstein, A. H., Quinn, P. K., Weber, R. J., and Worsnop, D. R. (2004a). Submicron Aerosol Composition at Trinidad Head, California, During ITCT 2K2: Its Relationship with Gas Phase Volatile Organic Carbon and Assessment of Instrument Performance. *J. Geophys. Res.–Atmos.* 109.

Allan, J. D., Delia, A. E., Coe, H., Bower, K. N., Alfarra, M. R., Jimenez, J. L., Middlebrook, A. M., Drewnick, F., Onasch, T. B., Canagaratna, M. R., Jayne, J. T., and Worsnop, D. R. (2004b). A Generalised Method for the Extraction of Chemically Resolved Mass Spectra from Aerodyne Aerosol Mass Spectrometer Data. *J. Aerosol. Sci.* 35:909–922.

Allan, J. D., Williams, P. I., Morgan, W. T., Martin, C. L., Flynn, M. J., Lee, J., Nemitz, E., Phillips, G. J., Gallagher, M. W., and Coe, H. (2010). Contributions from Transport, Solid Fuel Burning and Cooking to Primary Organic Aerosols in Two UK Cities. *Atmos. Chem. Phys.* 10:647–668.

Broekhuizen, K., Chang, R. Y. W., Leaitch, W. R., Li, S. M., and Abbatt, J. P. D. (2006). Closure Between Measured and Modeled Cloud Condensation Nuclei (CCN) Using Size-Resolved Aerosol Compositions in Downtown Toronto. *Atmos. Chem. Phys.* 6:2513–2524.

Canagaratna, M. R., Jayne, J. T., Ghertner, D. A., Herndon, S., Shi, Q., Jimenez, J. L., Silva, P. J., Williams, P., Lanni, T., Drewnick, F., Demerjian, K. L., Kolb, C. E., and Worsnop, D. R. (2004). Chase Studies of Particulate Emissions from In-Use New York City Vehicles. *Aerosol Sci. Technol.* 38:555–573.

Canagaratna, M. R., Jayne, J. T., Jimenez, J. L., Allan, J. D., Alfarra, M. R., Zhang, Q., Onasch, T. B., Drewnick, F., Coe, H., Middlebrook, A., Delia, A., Williams, L. R., Trimborn, A. M., Northway, M. J., DeCarlo, P. F., Kolb, C. E., Davidovits, P., and Worsnop, D. R. (2007). Chemical and Microphysical Characterization of Ambient Aerosols with the Aerodyne Aerosol Mass Spectrometer. *Mass Spectrometry Reviews* 26:185–222.

Chang, R. Y. W., Slowik, J. G., Shantz, N. C., Vlasenko, A., Liggio, J., Sjostedt, S. J., Leaitch, W. R., and Abbatt, J. P. D. (2010). The Hygroscopicity Parameter (kappa) of Ambient Organic Aerosol at a Field Site Subject to Biogenic and Anthropogenic Influences: Relationship to Degree of Aerosol Oxidation. *Atmos. Chem. Phys.* 10:5047–5064.

Cubison, M. J., Ervens, B., Feingold, G., Docherty, K. S., Ulbrich, I. M., Shields, L., Prather, K., Hering, S., and Jimenez, J. L. (2008). The Influence of Chemical Composition and Mixing State of Los Angeles Urban Aerosol on CCN Number and Cloud Properties. *Atmos. Chem. Phys.* 8:5649–5667.

de Gouw, J. A., Middlebrook, A. M., Warneke, C., Goldan, P. D., Kuster, W. C., Roberts, J. M., Fehsenfeld, F. C., Worsnop, D. R., Canagaratna, M. R., Pszenny, A. A. P., Keene, W. C., Marchewka, M., Bertman, S. B., and Bates, T. S. (2005). Budget of Organic Carbon in a Polluted Atmosphere: Results

Downloaded By: [Sun, Yele] At: 18:48 7 March 2011

Downloaded By: [Sun, Yele] At: 18:48 7 March 2011

from the New England Air Quality Study in 2002. *J. Geophys. Res.–Atmos.* 110:D16305, doi:16310.11029/12004JD005623.

DeCarlo, P. F., Kimmel, J. R., Trimborn, A., Northway, M. J., Jayne, J. T., Aiken, A. C., Gonin, M., Fuhrer, K., Horvath, T., Docherty, K., Worsnop, D. R., and Jiménez, J. L. (2006). A Field-Deployable High-Resolution Time-of-Flight Aerosol Mass Spectrometer. *Anal. Chem.* 78:8281–8289.

Docherty, K. S., Stone, E. A., Ulbrich, I. M., DeCarlo, P. F., Snyder, D. C., Schauer, J. J., Peltier, R. E., Weber, R. J., Murphy, S. M., Seinfeld, J. H., Grover, B. D., Eatough, D. J., and Jiimenez, J. L. (2008). Apportionment of Primary and Secondary Organic Aerosols in Southern California during the 2005 Study of Organic Aerosols in Riverside (SOAR–1). *Environ. Sci. Technol.* 42:7655–7662.

Drewnick, F., Jayne, J. T., Canagaratna, M., Worsnop, D. R., and Demerjian, K. L. (2004). Measurement of Ambient Aerosol Composition During the PMTACS-NY 2001 Using an Aerosol Mass Spectrometer. Part II: Chemically Speciated Mass Distributions. *Aerosol Sci. Technol.* 38:104–117.

Drewnick, F., Hings, S. S., DeCarlo, P., Jayne, J. T., Gonin, M., Fuhrer, K., Weimer, S., Jimenez, J. L., Demerjian, K. L., Borrmann, S., and Worsnop, D. R. (2005). A New Time-of-Flight Aerosol Mass Spectrometer (TOF-AMS)—Instrument Description and First field Deployment. *Aerosol Sci. Technol.* 39:637–658.

Herndon, S. C., Onasch, T. B., Wood, E. C., Kroll, J. H., Canagaratna, M. R., Jayne, J. T., Zavala, M. A., Knighton, W. B., Mazzoleni, C., Dubey, M. K., Ulbrich, I. M., Jimenez, J. L., Seila, R., de Gouw, J. A., de Foy, B., Fast, J., Molina, L. T., Kolb, C. E., and Worsnop, D. R. (2008). Correlation of Secondary Organic Aerosol with Odd Oxygen in Mexico City. *Geophys. Res. Lett.* 35:L15804, DOI:15810.11029/12008GL034058

Huang, X. F., He, L. Y., Hu, M., Canagaratna, M. R., Y., S., Q., Z., Zhu, T., Xue, L., Zeng, L. W., Liu, X. G., Zhang, Y. H., Jayne, J. T., Ng, N. L., and Worsnop, D. R. (2010). Highly Time-Resolved Chemical Characterization of Atmospheric Submicron Particles During 2008 Beijing Olympic Games Using an Aerodyne High-Resolution Aerosol Mass Spectrometer. *Atmos. Chem. Phys.*:8933–8945.

Huffman, J. A., Jayne, J. T., Drewnick, F., Aiken, A. C., Onasch, T., Worsnop, D. R., and Jimenez, J. L. (2005). Design, Modeling, Optimization, and Experimental Tests of a Particle Beam width Probe for the Aerodyne Aerosol Mass Spectrometer. *Aerosol Sci. Technol.* 39:1143–1163.

IPCC (2007). *Climate Change 2007: The Physical Scientific Basis*. Cambridge University Press, Cambridge, England.

Jayne, J. T., Leard, D. C., Zhang, X. F., Davidovits, P., Smith, K. A., Kolb, C. E., and Worsnop, D. R. (2000). Development of an Aerosol Mass Spectrometer for Size and Composition Analysis of Submicron Particles. *Aerosol Sci. Technol.* 33:49–70.

Jimenez, J. L., Jayne, J. T., Shi, Q., Kolb, C. E., Worsnop, D. R., Yourshaw, I., Seinfeld, J. H., Flagan, R. C., Zhang, X., Smith, K. A., Morris, J., and Davidovits, P. (2003). Ambient Aerosol Sampling Using the Aerodyne Aerosol Mass Spectrometer. *J. Geophys Res.* 108:8425 doi:8410.1029/2001JD001213.

Jimenez, J. L., Canagaratna, M. R., Donahue, N. M., Prevot, A. S. H., Zhang, Q., Kroll, J. H., DeCarlo, P. F., Allan, J. D., Coe, H., Ng, N. L., Aiken, A. C., Docherty, K. S., Ulbrich, I. M., Grieshop, A. P., Robinson, A. L., Duplissy, J., Smith, J. D., Wilson, K. R., Lanz, V. A., Hueglin, C., Sun, Y. L., Tian, J., Laaksonen, A., Raatikainen, T., Rautiainen, J., Vaattovaara, P., Ehn, M., Kulmala, M., Tomlinson, J. M., Collins, D. R., Cubison, M. J., Dunlea, E. J., Huffman, J. A., Onasch, T. B., Alfarra, M. R., Williams, P. I., Bower, K., Kondo, Y., Schneider, J., Drewnick, F., Borrmann, S., Weimer, S., Demerjian, K., Salcedo, D., Cottrell, L., Griffin, R., Takami, A., Miyoshi, T., Hatakeyama, S., Shimono, A., Sun, J. Y., Zhang, Y. M., Dzepina, K., Kimmel, J. R., Sueper, D., Jayne, J. T., Herndon, S. C., Trimborn, A. M., Williams, L. R., Wood, E. C., Middlebrook, A. M., Kolb, C. E., Baltensperger, U., and Worsnop, D. R. (2009). Evolution of Organic Aerosols in the Atmosphere. *Science* 326:1525–1529.

Kumar, P. P., Broekhuizen, K., and Abbatt, J. P. D. (2003). Organic Acids as Cloud Condensation Nuclei: Laboratory Studies of Highly Soluble and Insoluble Species. *Atmos. Chem. Phys.* 3:509–520.

Lanz, V. A., Alfarra, M. R., Baltensperger, U., Buchmann, B., Hueglin, C., and Prévôt, A. S. H. (2007). Source Apportionment of Submicron Organic Aerosols at an Urban Site by Factor Analytical Modelling of Aerosol Mass Spectra. *Atmos. Chem. Phys.* 7:1503–1522.

Liu, P., Ziemann, P. J., Kittelson, D. B., and McMurry, P. H. (1995a). Generating Particle Beams of Controlled Dimensions and Divergence .1. Theory of Particle Motion in Aerodynamic Lenses and Nozzle Expansions. *Aerosol Sci. Technol.* 22:293–313.

Liu, P., Ziemann, P. J., Kittelson, D. B., and McMurry, P. H. (1995b). Generating Particle Beams of Controlled Dimensions and Divergence .2. Experimental Evaluation of Particle Motion in Aerodynamic Lenses and Nozzle Expansions. *Aerosol Sci. Technol.* 22:314–324.

Liu, P. S. K., Deng, R., Smith, K. A., Williams, L. R., Jayne, J. T., Canagaratna, M. R., Moore, K., Onasch, T. B., Worsnop, D. R., and Deshler, T. (2007). Transmission Efficiency of an Aerodynamic Focusing Lens System: Comparison of Model Calculations and Laboratory Measurements for the Aerodyne Aerosol Mass Spectrometer. *Aerosol Sci. Technol.* 41:721–733.

Massoli, P., Lambe, A. T., Ahern, A. T., Williams, L. R., Ehn, M., Mikkila, J., Canagaratna, M. R., Kulmala, M., Onasch, T. B., Brune, W., Jayne, J. T., Worsnop, D. R., Kolb, C. E., and Davidovitis, P. (2010). Relationship Between Aerosol Oxidation Level and Hygroscopic Properties of Laboratory Generated Secondary Organic Aerosols (SOA). *Geophys. Res. Lett.*:In press.

Matthew, B. M., Middlebrook, A. M., and Onasch, T. B. (2008). Collection Efficiencies in an Aerodyne Aerosol Mass Spectrometer as a Function of Particle Phase for Laboratory Generated Aerosols. *Aerosol Sci. Technol.* 42:884–898.

Ng, N. L., Canagaratna, M. R., Zhang, Q., Jimenez, J. L., Tian, J., Ulbrich, I. M., Kroll, J. H., Docherty, K. S., Chhabra, P. S., Bahreini, R., Murphy, S. M., Seinfeld, J. H., Donahue, N. M., Hildebrandt, L., Decarlo, P. F., Lanz, V. A., Prevot, A. S. H., Dinar, E., Rudich, Y., and Worsnop, D. R. (2010). Organic Aerosol Components Observed in Worldwide Datasets from Aerosol Mass Spectrometry. *Atmos. Chem. Phys.* 10:4625–4641.

Paatero, P. (2008). Interactive Comment on "Interpretation of Organic Components from Positive Matrix Factorization of Aerosol Mass Spectrometric Data" by I. M. Ulbrich et al. *Atmospheric Chemistry and Physics Discussions* 8:S2059–S2068.

Pope, C. A., and Dockery, D. W. (2006). Health Effects of Fine Particulate Air Pollution: Lines That Connect. *J. Air Waste Manage. Assoc.* 56:709–742.

Pöschl, U. (2005). Atmospheric Aerosols: Composition, Transformation, Climate and Health Effects. *Angewandte Chemie–International Edition* 44:7520–7540.

Quinn, P. K., Bates, T. S., Coffman, D. J., and Covert, D. S. (2008). Influence of Particle Size and Chemistry on the Cloud Nucleating Properties of Aerosols. *Atmos. Chem. Phys.* 8:1029–1042.

Raymond, T. M., and Pandis, S. N. (2002). Cloud Activation of Single–Component Organic Aerosol Particles. *J. Geophys. Res.–Atmos.* 107.

Schwab, J. J., Hogrefe, O., Demerjian, K. L., Dutkiewicz, V. A., Husain, L., Rattigan, O. V., and Felton, H. D. (2006). Field and Laboratory Evaluation of the Thermo Electron 5020 Sulfate Particulate Analyzer. *Aerosol Sci. Technol.* 40:744–752.

Sun, Y. L., Zhang, Q., Schwab, J. J., Demerjian, K. L., Chen, W. N., Bae, M. S., Hung, H. M., Hogrefe, O., Frank, B., Rattigan, O. V., and Lin, Y. C. (2010). Characterization of the Sources and Processes of Organic and Inorganic Aerosols in New York City With a High-Resolution Time-Of-Flight Aerosol Mass Spectrometer. *Atmos. Chem. Phys. Discuss.* 10:22669–22723.

Ulbrich, I. M., Canagaratna, M. R., Zhang, Q., Worsnop, D. R., and Jimenez, J. L. (2009). Interpretation of Organic Components from Positive Matrix Factorization of Aerosol Mass Spectrometric Data. *Atmos. Chem. Phys.* 9:2891–2918.

Volkamer, R., Jimenez, J. L., San Martini, F., Dzepina, K., Zhang, Q., Salcedo, D., Molina, L. T., Worsnop, D. R., and Molina, M. J. (2006). Secondary Organic Aerosol Formation from Anthropogenic Air Pollution: Rapid and Higher Than Expected. *Geophys. Res. Lett.* 33:L17811, doi:17810.11029/12006GL026899.

Weber, R. J., Orsini, D., Daun, Y., Lee, Y. N., Klotz, P. J., and Brechtel, F. (2001). A Particle-Into-Liquid Collector for Rapid Measurement of Aerosol Bulk Chemical Composition. *Aerosol Sci. Technol.* 35:718–727.

Werle, P., Mucke, R., and Slemr, F. (1993). The Limits of Signal Averaging in Atmospheric Trace-Gas Monitoring by Tunable Diode-Laser Absorption-Spectroscopy (Tdlas). *Applied Physics B–Photophysics and Laser Chemistry* 57:131–139.

Zhang, Q., Alfarra, M. R., Worsnop, D. R., Allan, J. D., Coe, H., Canagaratna, M. R., and Jimenez, J. L. (2005a). Deconvolution and Quantification of Hydrocarbon-Like and Oxygenated Organic Aerosols Based on Aerosol Mass Spectrometry. *Environ. Sci. Technol.* 39:4938–4952.

Zhang, Q., Canagaratna, M. R., Jayne, J. T., Worsnop, D. R., and Jimenez, J. L. (2005b). Time- and Size-Resolved Chemical Composition of Submicron Particles in Pittsburgh: Implications for Aerosol Sources and Processes. *J. Geophys. Res.–Atmos.* 110.

Zhang, Q., Jimenez, J. L., Canagaratna, M. R., Allan, J. D., Coe, H., Ulbrich, I., Alfarra, M. R., Takami, A., Middlebrook, A. M., Sun, Y. L., Dzepina, K., Dunlea, E., Docherty, K., DeCarlo, P. F., Salcedo, D., Onasch, T., Jayne, J. T., Miyoshi, T., Shimono, A., Hatakeyama, S., Takegawa, N., Kondo, Y., Schneider, J., Drewnick, F., Borrmann, S., Weimer, S., Demerjian, K., Williams, P., Bower, K., Bahreini, R., Cottrell, L., Griffin, R. J., Rautiainen, J., Sun, J. Y., Zhang, Y. M., and Worsnop, D. R. (2007). Ubiquity and Dominance of Oxygenated Species in Organic Aerosols in Anthropogenically–Influenced Northern Hemisphere Midlatitudes. *Geophys. Res. Lett.* 34:L13801, doi:13810.11029/12007GL029979.

Downloaded By: [Sun, Yele] At: 18:48 7 March 2011